Journal of Sustainable Cement-Based Materials

ISSN: (Print) (Online) Journal homepage: https://www.tandfonline.com/loi/tscm20

Investigation of the effect of diethanol isopropanolamine on ferrite phase

Hyunuk Kang, Sungjin Jung, Junhyeok Jung, Jungwon Park, Jun-Boum Park & Juhyuk Moon

To cite this article: Hyunuk Kang, Sungjin Jung, Junhyeok Jung, Jungwon Park, Jun-Boum Park & Juhyuk Moon (2023): Investigation of the effect of diethanol isopropanolamine on ferrite phase, Journal of Sustainable Cement-Based Materials, DOI: 10.1080/21650373.2023.2248487

To link to this article: https://doi.org/10.1080/21650373.2023.2248487

Journal of Sustainable Cement-Based Materials, 2023
http://dx.doi.org/10.1080/21650373.2023.2248487

Investigation of the effect of diethanol isopropanolamine on ferrite phase

Hyunuk Kang[a], Sungjin Jung[a], Junhyeok Jung[c], Jungwon Park[c,d,e,f], Jun-Boum Park[a,b] and Juhyuk Moon[a,b]*

[a]*Department of Civil and Environmental Engineering, Seoul National University, Seoul, Republic of Korea;* [b]*Institute of Construction and Environmental Engineering, Seoul, Republic of Korea;* [c]*School of Chemical and Biological Engineering, Institute of Chemical Processes, Seoul National University, Seoul, Republic of Korea;* [d]*Center for Nanoparticle Research, Institute for Basic Science (IBS), Seoul, Republic of Korea;* [e]*Institute of Engineering Research, College of Engineering, Seoul National University, Seoul, Republic of Korea;* [f]*Advanced Institutes of Convergence Technology, Seoul National University, Gyeonggi-do, Republic of Korea*

Although it is one of main cement phases, the reactivity of tetracalcium aluminoferrite (C_4AF) has not been fully understood especially under the use of grinding agent. In this study, the crystallographic variations due to the use of diethanol isopropanolamine (DEIPA) and resulting hydration characteristics of iron-rich $C_4A_{0.6}F_{1.4}$ (f-C_4AF) and idealized $C_4A_{0.8}F_{1.2}$ (i-C_4AF) were investigated. Substantially enhanced reactivity of f-C_4AF was confirmed due to the state variation of Fe atom in C_4AF from Fe^{2+} to Fe^{3+} which facilitates the formation of Fe-bearing phases of C_3FH_6, Fe-AFm and FH_3. Meanwhile, the degree of hydration of i-C_4AF had not been substantially improved but showed similar reaction only with a large amount of DEIPA (from 0.1% to 0.3%). It was experimentally validated that the reactivity of C_4AF is controllable with the use of DEIPA which can lead to develop sustainable cement such as ferrite rich Portland cement.

Keywords: X-ray diffraction method; diethanol isopropanolamine; tetracalcium aluminoferrite; hydration mechanism

1. Introduction

Tetracalcium aluminoferrite (C_4AF) is the main clinker phase of Portland cement (PC), which is a complex solid solution phase of $Ca_2Fe_{2-x}Al_xO_5$ ($0 \leq x \leq 1.4$) [1–3]. Although the C_4AF phase is around 5–15 wt.% contained in the PC, it does not participate in cement hydration reactions as much as other clinker phases [4–6]. Nevertheless, ferrite-rich PC (FRPC) with high C_4AF content can serve as an oil well PC owing to its excellent sulfate resistance [7]. Moreover, as FRPC is useful in the treatment of materials and industrial by-products that are rarely used for supplementary cementitious materials, it has been highlighted as sustainable PC with price competitiveness [6, 8, 9]. However, as mentioned above, it has been well known that the FRPC delays the development of mechanical properties owing to the relatively low reactivity of C_4AF [9,10]. Therefore, considering the potential of FRPC to be applicated in multiple fields, research on how to enhance the reactivity of C_4AF is essential.

To enhance the functionality of FRPC, various efforts are being conducted. To that end, a grinding agent (GA) could be added to the PC at the grinding stage [11–14]. Using this process, not only was the grinding efficiency of PC enhanced, which can play a positive role in terms of energy savings [15,16], but the hydration reaction of the clinker phases was also dramatically improved with the GA [10, 17–19]. For example, with triethanolamine (TEA), an enhanced aluminate reactions (aluminate [C_3A] and C_4AF) was reported compared to the reference sample, which was suggested to have a significant impact on the mechanical performance of the concrete [20]. Gartner et al. reported that triisopropanolamine (TIPA) can promote the hydration of C_4AF even after the sulfate exhaustion point, and it suggested that the effects might enhance the later stage (28 days) of compressive strength of concrete [10]. In the case of diethanol isopropanolamine (DEIPA), the reaction of C_4AF during the aluminate reactions was accelerated within 24 h. It was concluded that the increased hydration degree of PC was closely related to the aforementioned effects [19].

As summarized, TIPA-based GA had a significant effect on PC hydration [10, 19, 21]. In particular, previous studies have confirmed that DEIPA acts as a catalyst in which the Fe atom constituting the C_4AF phase actively participates in the PC hydration reaction [19]. It could suggest that the reactivity of C_4AF enhanced by DEIPA produced more Fe-bearing hydration products (i.e. AFt, AFm, and C-S-H phases), which increased the overall hydration degree of PC. However, more in-depth studies on the effects of the DEIPA on the hydration mechanism of C_4AF have not yet been conducted. It includes the effects of the type of solid solution phase, Fe/Al ratio in C_4AF, the dosage of the DEIPA as well as the direct evidence of the improved reactivity of C_4AF such as ion state of Fe atom.

Therefore, the aim of this study is to elucidate the effects of dosages (0, 0.1 and 0.3 wt.%) of DEIPA on the crystallographic variations in the 2 types of C_4AF phases (iron-rich $C_4A_{0.6}F_{1.4}$ [f-C_4AF] and idealized $C_4A_{0.8}F_{1.2}$ [i-C_4AF]). It also includes the experimental evidence of the

*Corresponding author. Email: juhyukmoon@snu.ac.kr

enhanced hydration mechanism of C_4AF caused by the crystallographic modifications. A fundamental investigation was conducted on the crystallographic variations of C_4AF induced by DEIPA using X-ray diffraction (XRD), transmission electron microscopy (TEM), inductively coupled plasma optical emission spectroscopy (ICP-OES), and X-ray photoelectron spectroscopy (XPS). Furthermore, isothermal calorimetry, thermogravimetric analysis (TGA), and quantitative XRD (QXRD) were used to investigate the hydration properties.

2. Materials and experimental methods

2.1. Sample preparation

For this study, two types of C_4AF were synthesized using calcium carbonate ($CaCO_3$; WAKO Co. Ltd., Richmond, CA, USA), aluminum oxide (Al_2O_3; Samchun Co. Ltd., Gyeonggi-do, Republic of Korea), and iron oxide (Fe_2O_3; Samchun Co. Ltd.). The target ratios of Fe-to-Al atoms in the i-C_4AF and f-C_4AF were set to 1.0 and 3.0, respectively. The i-C_4AF mix contained 823.80 g $CaCO_3$, 209.82 g Al_2O_3, and 328.61 g Fe_2O_3, while the f-C_4AF contained 777.62 g $CaCO_3$, 99.03 g Al_2O_3, and 465.27 g Fe_2O_3. These were mixed for 10 min in a mortar mixer, and subsequently, the heating rate was set to 14.4 °C per minute for 90 min. Afterward, the temperature was held at 1,300 °C for 2 h. Finally, the mixtures were quenched [22].

The pre-processing method of C_4AF used in this experiment was as follows: First, C_4AF nodules were manufactured using the process already described. Subsequently, coarse C_4AF powders were obtained by hand grinding for 5 min. Using the powder thus obtained, the oxide compositions of i-C_4AF and f-C_4AF were measured by X-ray fluorescence (S8 Tiger, Bruker Co. Ltd., Land Baden-Württemberg, Germany), and the results are provided in Table 1. The QXRD results of f-C_4AF and i-C_4AF were shown in Table 2. The pure DEIPA was provided by a commercial company (SilkroadC&T, Seoul, Korea). Samples of f-C_4AF and i-C_4AF series were distinguished by the DEIPA contents (0.1 and 0.3 wt.%) added before the grinding procedure (Table 3). The water-to-C_4AF ratio for paste was set to 0.5. Subsequently, the C_4AF paste was enclosed and underwent curing within a 20 °C environment for the initial day. Following this, it was demolded and then subjected to curing within an environment with both a temperature of 20 °C and a relative humidity of 95% or higher.

Table 1. X-ray fluorescence results of tests on C_4AF powders.

Phases	f-C_4AF (unit %)	i-C_4AF (unit %)
Fe_2O_3	47.44	36.68
CaO	43.28	46.80
Al_2O_3	8.47	16.00
SiO_2	0.41	0.25
MgO	0.18	0.09
MnO	0.11	0.09
Cr_2O_3	0.04	–
SrO	0.03	0.04
Cl	0.03	–
CuO	0.01	–

2.2. Experimental method

2.2.1. Selected grinding program

Micro ball mill equipment (McCrone Micronizing Mill; McCrone Scientific Ltd., London, UK) with a 125 ml jar and 48 cylindrical grinding balls was used to grind the C_4AF powder. Several preliminary tests were performed to reproduce the final cement grinding program, where 10 grams of C_4AF powder with the specified amount of DEIPA were ground under the 14 min of grinding time and 1,166 rpm rotation speed.

2.2.2. Particle size measurements

Particle size distribution was measured with a microparticle size analyzer (Malvern Instruments Ltd., Malvern, UK). Isopropyl alcohol was used as the dispersion medium to prevent the hydration reaction of C_4AF [23]. The results thus obtained were used to investigate the effects of DEIPA on the grinding performance of C_4AF powder.

2.2.3. TEM measurements

Morphological analysis was conducted using a TEM (JEM-2100F; JEOL Ltd., Tokyo, Japan) equipped with an UltraScan 1000XP CCP detector, and voltage generation was set at 200 kV [24]. The TEM measurement process was as follows: The dispersion method with a sonicator was used for dispersing the powders and obtaining a single particle. The chosen dispersion medium was a hexane solution that does not react with DEIPA. In that process, a 5 μm particle was selected and placed in a carbon-coated Cu TEM grid. Lastly, the measurement space was vacuumed for a few minutes before the measurement [25].

Table 2. QXRD results of unhydrated f-C_4AF and i-C_4AF.

Phase	f-C_4AF	i-C_4AF
f-C4AF	99.1	–
i-C4AF	–	95.1
Calcium oxide	0.9	2.0
Calcium carbonate	–	2.9

Table 3. Mix design for unhydrated C_4AF powder. (before grinding program).

Sample label	f-C_4AF	i-C_4AF	DEIPA
f-C_4AF_0%	100	–	–
f-C_4AF_0.1%	100	–	0.1
f-C_4AF_0.3%	100	–	0.3
i-C_4AF_0%	–	100	–
i-C_4AF_0.1%	–	100	0.1
i-C_4AF_0.3%	–	100	0.3

2.2.4. XPS measurements

An AXIS Supra + spectrometer for chemical analysis (Kratos Analytical Limited, Manchester, UK) was used to measure XPS patterns of selected samples of f-C_4AF_0% and _0.3%. The binding energy range was set at 0–1,200 eV with a data rate of 1 point per eV [26]. The powders were completely dried for 1 day in a vacuum environment at ambient temperature. Next, the measurement sample was formed into a 7 mm diameter pressed pellet. The analysis was adopted to observe the variations in the speciation of Fe atoms depending on the DEIPA that was added. The analysis of XPS spectra was conducted using XPSPEAK 4.1 software, which was also used for the relative quantitative analysis of XPS. A Shirley type background was chosen for the XPS spectra due to the complexity. The peak position, area, and full width at half maximum (FWHM) parameters were fitted based on the function of the Gaussian–Lorentzian ratio (3:2) [27].

2.2.5. ICP-OES measurements

ICP-OES measurements were performed with an Agilent 5100 SVDV ICP-OES (Agilent Technologies, Santa Clara, CA, USA). For the ICP-OES measurements, the pure water-to-C_4AF ratio was set to 10:1 by weight. After stirring for 30 min, the solutions were filtered through a 200 nm filter. Before starting the measurement, the plasmid argon gas was obtained by an induction magnetic field, and a preprocessed liquid was sprayed into the particles and injected [28].

2.2.6. Isothermal calorimetry measurements

The exothermic processes of C_4AF hydration were measured by the micro-calorimeter (TAM Air 8-channel, TA Instruments, New Castle, DE, USA). The water-to-C_4AF was assigned as 1:2 by weight. Before starting the experiment, the equipment was calibrated by maintaining a constant temperature in a 20 °C environment for at least 24 h. After the water (4 g) and C_4AF powder (8 g) were mixed for 2 min, the 6 grams of the slurry was inserted into the equipment. The results of heat flow and cumulative heat measurements were normalized to the amount of the C_4AF powder contained in the ampule.

2.2.7. XRD measurements

XRD patterns were obtained with a D2 PHASER X-ray diffractometer (Bruker Co. Ltd., Land Baden-Württemberg, Germany) equipped with Cu-Kα radiation ($\lambda = 1.5418$ Å). The generator voltage and tube current were set at 30 kV and 10 mA, respectively [29,30]. The hydration stop method was used with the samples that were hydrated for 5 days. First, the hardened paste sample was pulverized for 10 min to obtain fine powders. Next, to remove any free water still contained in a hydrated paste, isopropyl alcohol and diethyl ether, respectively, were used as exchange solutions [31,32].

The measured XRD patterns of the powders were analyzed using TOPAS software version 7.0 (Bruker Co. Ltd., Land Baden-Württemberg, Germany). The background of XRD patterns was assigned using the Chebyshev polynomial and 1/X terms in TOPAS software. To create the C_4AF models, the scale factors, lattice parameters, and FWHM parameters were refined with an XRD pattern [33,34]. The occupancy factors of Fe^{3+} and Al^{3+} atoms were also refined in this process [35].

To quantitatively analyze the hydrated paste, an internal standard method was adopted in the QXRD. C_4AF powder and an internal standard reference were mixed with a certain weight ratio (1:9) using hand mixing for 30 min [32, 36,37]. The Al_2O_3 (NIST SRM 676a) internal standard reference, which does not overlap with the other phases, was adopted. The reference crystal structures adopted to analyze the XRD pattern were presented in Table 4. In addition, $C_3(A, F)H_6$ phases were observed in all hydrated C_4AF [44,45]. However, it is challenging to elucidate the ratio of Al/Fe atoms contained in the $C_3(A, F)H_6$ phase [7, 45]. Therefore, qualitative analysis was performed assuming that only C_3FH_6 and C_3AH_6 existed in the $C_3(A, F)H_6$ phases.

Next, all phases for which quantitative analyses were to be conducted were completed using the Rietveld refinement method. Then, the contents of the quantified phases were corrected with the amount of internal standard reference added by Equation (1). In the case of amorphous content, the added amount of internal standard was calculated and presented in a proportional manner. Finally, the weight percentage of each phase was corrected considering the chemically bound water (CBW) amount, which was the weight loss at 600 °C was assigned, from the TGA results (Equation (2)). In details, the value obtained by subtracting the quantity of CBW from the initially mixed water content with C_4AF was regarded as the amount of free water. Therefore, the actual amount of minerals in the hydrated C_4AF paste considering free water content can be compared [31].

$$Corr(w_\alpha) = w_\alpha \frac{STD_{known}}{STD_{measured}} \quad (1)$$

$$w_{amorphous} = 1 - \sum_{j=1}^{n} Corr(w_j) \quad (2)$$

where w_α, $Corr(w_\alpha)$, STD_{known}, and $STD_{measured}$ indicate the weight percentage of α, corrected weight percentage of α, weight concentration of internal standard reference, and analyzed concentration of internal standard reference, respectively.

2.2.8. TGA measurements

A differential scanning calorimeter (DSC)–TG system (SDT Q600, TA Instruments Ltd., Newcastle, DE, USA) was chosen to measure the TGA. The heating rate was 10 °C per minute, and the measured range was 30 °C–1,000 °C [31]. At 5 days, all sample investigations were also conducted through the hydration stop process, and 25–30 mg of powder was measured to analyze the degree of hydration in each sample.

Table 4. Used COD database information.

Phase	Database	Reference
C_4AF (Ca_4AlFeO_7)	COD 1200009	[38]
Al-hydrogarnet ($Ca_3Al_2(OH)_{12}$)	COD 1531652	[39]
Monocarbonate ($Ca_4Al_2(CO_3)_{0.5}(OH)_{13}\cdot 5.5H_2O$)	COD 1000459	[40, 41]
Hemicarbonate ($Ca_4Al_2(CO_3)(OH)_{12}\cdot 5H_2O$)	COD 2105252	[42]
Gibbsite ($Al(OH)_3$)	COD 1200016	[43]

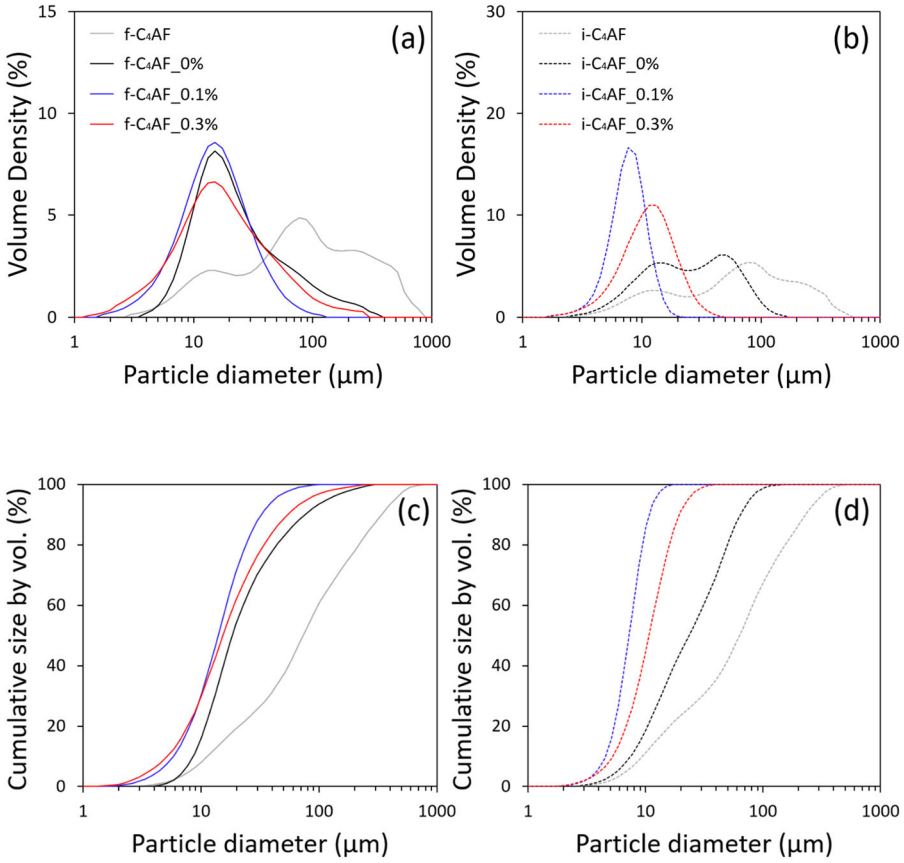

Figure 1. Particle size distributions of (a and c) f-C_4AF and (b and d) i-C_4AF.

3. Results

3.1. Particle size distribution

As shown in Figure 1(a–d), the particle size distributions and cumulative curves of the i-C_4AF and f-C_4AF powder are presented according to the amount of DEIPA added. The particle size distribution of raw C_4AF particles shows wide range. For f-C_4AF sample, particles ranging from 2.6 to 890.1 μm were observed, while in the case of i-C_4AF sample, particles ranging from 2.60 to 592.4 μm were confirmed. Interestingly, regardless of the type of C_4AF, the grindability was significantly enhanced with the DEIPA dosage of 0.1 wt.% under the same grinding condition. But, when the amount of added DEIPA was to 0.3 wt.%, the grindability was slightly decreased, as compared to the sample with that of 0.1 wt.%. These results are similar to a previous study finding that when excessive amounts of GA were applied to PC, the mixture exhibited poor grindability [46]. It should be noted here that a menial effect on particle size reduction was observed with C_4AF_0.3%, as compared to the sample of C_4AF_0.1%. The differences in grindability between the two can be explained as follows: In the case of C_4AF_0.1%, a substantial amount of energy induced by the grinding contributed to the particle size reduction. However, with the C_4AF_0.3%, the high-volume energy induced by the selected grinding program might have mainly affected the crystallographic properties (i.e. unit cell parameters and bond length) [23, 47].

3.2. XPS results

The XPS measurement results are presented in Figure 2. According to the sample type, variations were observed in the XPS spectra. In particular, a significant change was observed in the scan range of 702 eV to 726 eV, which is closely related to Fe atoms [26, 48]; the peaks at 706 eV and 708 eV indicate Fe^{3+}, and the Fe^{2+} peak is at 714 eV [49–51]. With the f-C_4AF_0%, the peaks corresponding to Fe^{2+} and Fe^{3+} ions were measured to be relatively higher than those for f-C_4AF_0.3%. However, as the relative ratio of the Fe^{2+} and Fe^{3+} peaks should be considered, detailed explanations for this phenomenon will be provided later.

3.3. ICP-OES results

The ICP-OES results are provided in Figure 3(a,b). The method was adopted to elucidate the reactivity of Ca, Al, and Fe atoms contained in C_4AF phase. When the amount of DEIPA was increased, an increased total ion count was confirmed. In particular, the elution of Fe ions was 0 ppm with f-C_4AF_0% and i-C_4AF_0% samples, but the detected Fe ions were significantly increased with the DEIPA application. When DEIPA was not added, the reactivity of each atom was in the order of Ca, Al, and Fe atoms [2]. However, the order of reactivity changed with f-C_4AF_0.3% and i-C_4AF_0.3% to the order of Ca, Fe, and Al atoms. This tendency was conspicuously observed in f-C_4AF compared to i-C_4AF. These indicate that there is strong support for DEIPA acting as a catalyst to enhance the reactivity of Fe ions contained in C_4AF.

3.4. Calorimetric results

As shown in Figure 4(a), the effect of DEIPA (dosages of 0.1 and 0.3%) on C_4AF hydrations was obtained. Once the water and C_4AF come into contact, a significant amount of heat was released and the effect continued for 24 h. And then, the hydration reaction of all C_4AF investigated was almost completed within 4 days; after 4 days, the released heat of all samples converged to about 0.08 mW/g.

In more detail, until 6 h, the i-C_4AF_0% sample had a higher amount of released heat, but after that, a larger amount of hydration heat was released from the DEIPA-added i-C_4AF samples (Figure 5(b)). Subsequently, the cumulative heat at 100 h was almost similar for all i-C_4AF series. Meanwhile, for f-C_4AF series, a different trend was observed. As the amount of DEIPA was increased, the initial hydration reaction was accelerated and enhanced, and this trend was maintained until 100 h. From these results, it was confirmed that DEIPA not only accelerated the initial hydration reaction of C_4AF but also improved the overall degree of hydration (in particular, f-C_4AF series).

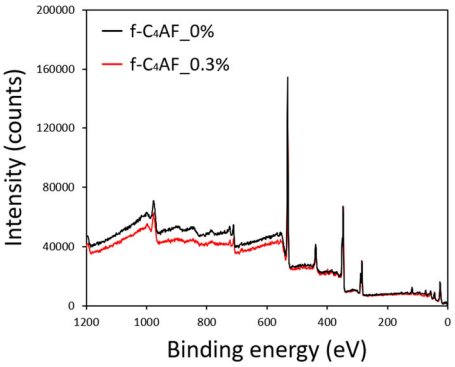

Figure 2. XPS measurements of f-C_4AF series.

3.5. TGA results

As mentioned above, the weight loss at 600 °C was assigned as CBW [31]. With these values, the degree of hydration reaction was determined to be different according to not only the type of C_4AF used but also amount of DEIPA added (Table 5). With the DEIPA, the degree of hydration reaction was significantly increased in the f-C_4AF series. However, in the case of the i-C_4AF series, a similar degree of hydration reaction was observed regardless of DEIPA added. These results indicated that the reactivity of f-C_4AF, which contains more amount of Fe atoms, was significantly improved, and it can be concluded that the Fe atoms contribute remarkably to the hydration reaction by the catalytic behavior of DEIPA.

More specially, as shown in Figure 5(a–d), hydrated C_4AF pastes experience a range of decomposition of minerals as the temperature increases. In our study, the range for weight loss of 110 °C to 180 °C indicated the decomposition of Fe-hemicarbonate (Fe-Hc, $Ca_4Fe_2(CO_3)_{0.5}(OH)_{12}\cdot 4H_2O$), and the decomposition temperatures of Fe-monocarbonate (Fe-Mc, $Ca_4Fe_2(CO_3)(OH)_{12}\cdot 6H_2O$) and Al-monocarbonate (Al-Mc, $Ca_4Al_2(CO_3)(OH)_{12}\cdot 5H_2O$) were below 240 °C [40]. The major weight loss between 250 °C and 280 °C could be attributed to the phases of gibbsite (AH_3), FeOOH, and iron hydroxide (FH_3) decomposition [52–55]. Based on these previous studies, it is possible to predict the hydration properties of all the hydrated samples studied. That is, the hydration mechanism of i-C_4AF_0.3% was remarkably modified compared to i-C_4AF_0% and i-C_4AF_0.1%. As a result, in the case of i-C_4AF_0.3%, it was measured similarly to the TGA results of the f-C_4AF

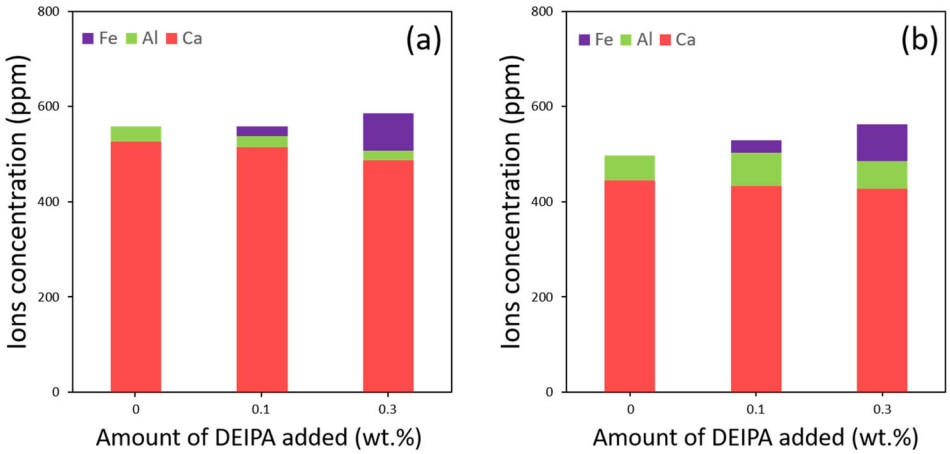

Figure 3. ICP-OES measurements of (a) f-C_4AF and (b) i-C_4AF.

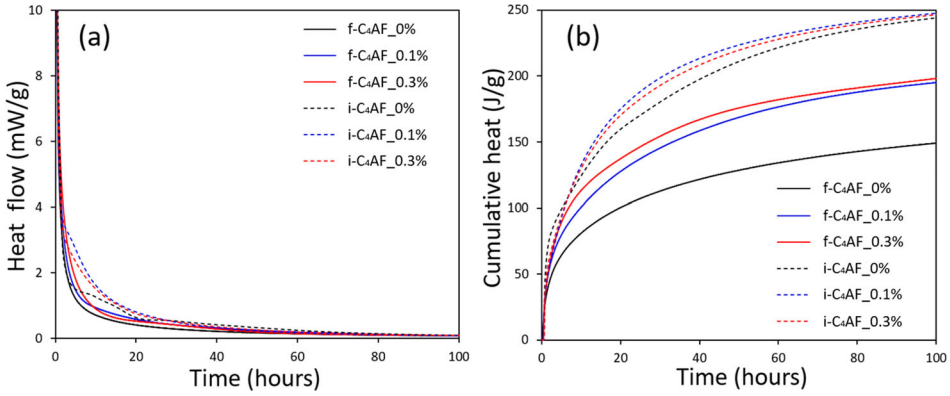

Figure 4. Hydration heat evolution of the slurry of C_4AF and water containing DEIPA: (a) heat flow results and (b) cumulative heat results.

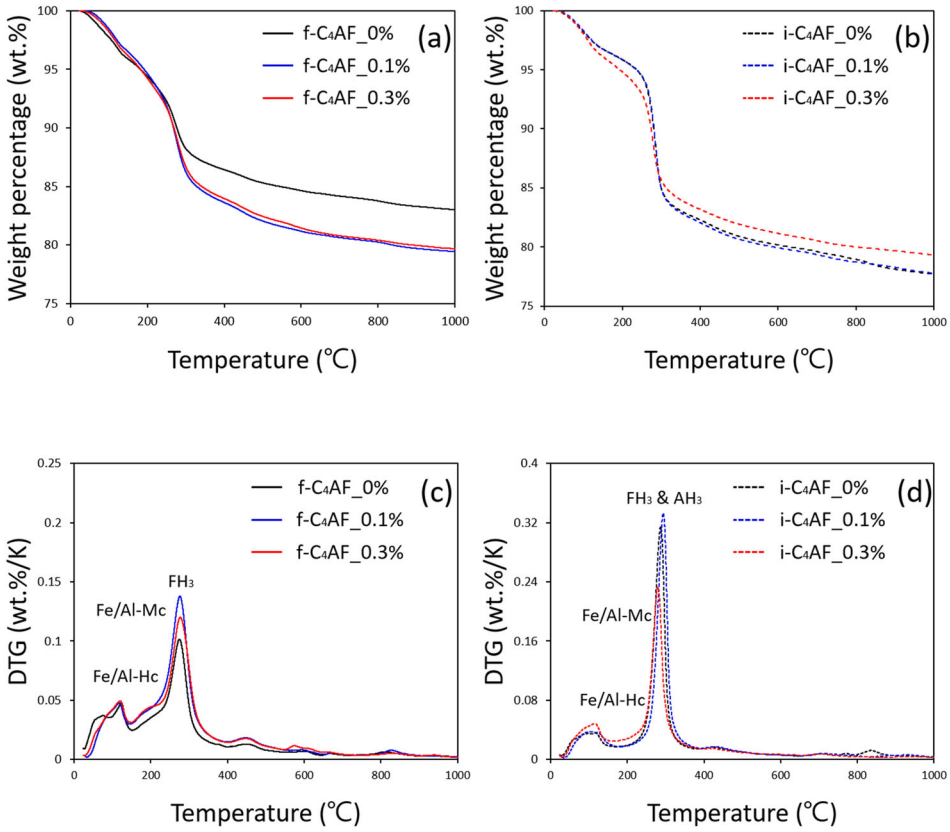

Figure 5. Results of TG and its derivative curves of (a and c) f-C_4AF and (b and d) i-C_4AF cured for 5 days.

Table 5. CBW value of C_4AF cured for 5 days.

Sample label	CBW (wt.%)	Sample label	CBW (wt.%)
i-C_4AF_0%	19.8	f-C_4AF_0%	15.4
i-C_4AF_0.1%	20.1	f-C_4AF_0.1%	18.8
i-C_4AF_0.3%	18.8	f-C_4AF_0.3%	18.6

series. It revealed that the reactivity of i-C_4AF was only enhanced with a large amount of DEIPA (dosage of 0.3%), resulting in a significant amount of Fe-containing hydration products.

3.6. *XRD results*

The obtained XRD patterns of the unhydrated C_4AF are shown in Figure 6(a–f). With the samples of f-C_4AF_0% and i-C_4AF_0%, the relative intensity of XRD peaks differed. As mentioned, this discrepancy was caused by the different ratios of Fe and Al atoms constituting C_4AF, so unit cell parameters, FWHM, and Fe/Al ratio were refined (Figure 6(a–b)). Surprisingly, according to the DEIPA added, the XRD pattern of C_4AF was greatly changed at the peaks of 12°, 32°, 33.5°, and 34° in the 2θ axis (Figure 6(c–f)). In addition, Figure 7(a–f) presented the fitting results of all samples cured for 5 days. A difference was confirmed in the hydration degree of f-C_4AF with the addition of DEIPA. Meanwhile, the difference was negligible in the case of i-C_4AF series. The detailed analysis approaches of crystallographic variations and the detailed explanations of the difference in hydration mechanism induced by DEIPA will be discussed in discussion session.

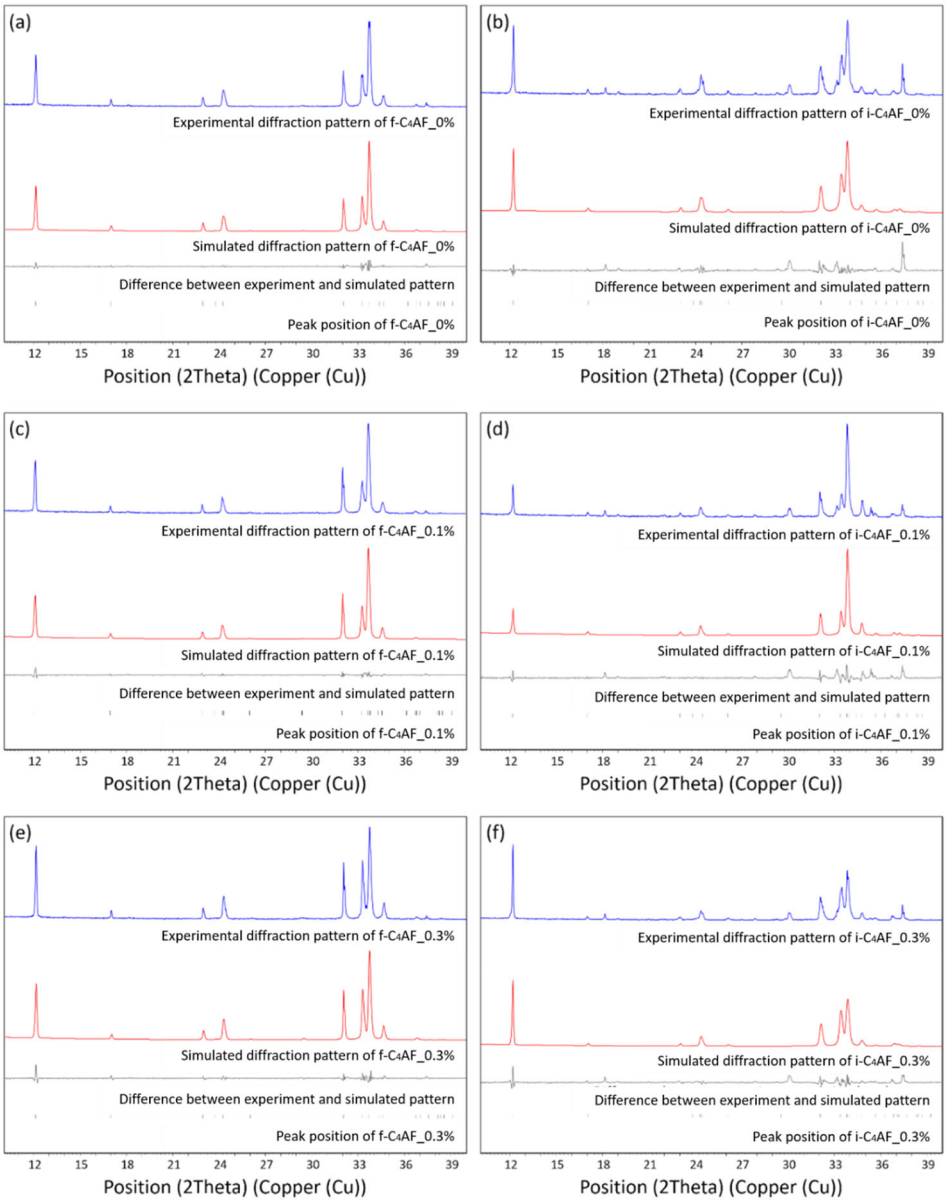

Figure 6. X-ray diffraction patterns of the investigated C_4AF according to the amount of DEIPA added and the created X-ray diffraction models of C_4AF: (a) f-C_4AF_0%, (b) i-C_4AF_0%, (c) f-C_4AF_0.1%, (d) i-C_4AF_0.1%, (e) f-C_4AF_0.3%, and (f) i-C_4AF_0.3%.

4. Discussion

4.1. *Effects of DEIPA on morphological characteristics of C_4AF*

High-resolution TEM images (Figure 8(a–l)) allows to examine the surface morphology of the C_4AF particle. It was observed that the substances considered to be DEIPA were attached to the particle surface of f-C_4AF_0.3% (Figure 8(c)). The EDS results support the aforementioned phenomenon. In the samples of the f-C_4AF_0%, the Ca, Fe, and Al atoms that are the major constituents of C_4AF were significantly observed (Figure 8(d)). However, the detected amount of these major constituents decreased as the amount of DEIPA increased, but that of carbon increased (Figure 8(d–f)).

Meanwhile, there was no clear trend in the case of i-C_4AF. The surface of i-C_4AF_0% looks completely different from those of f-C_4AF series. It can be due to the better grindability of the material due to the low amount of Fe content. Although the carbon content was increased with the increase of DEIPA, there was no substantial difference in terms of surface morphology of the i-C_4AF.

4.2. *Observation of crystallographic variations in C_4AF induced by DEIPA*

As shown in Figure 9(a–d), significant changes of XRD pattern were observed in the f-C_4AF and i-C_4AF due to the addition of DEIPA. Firstly, the nanocrystalline size particle could be generated which yields the reduction of the area of XRD peaks [56,57]. However, this explanation might not be suitable for the present study, as the grinding process has been chosen to reproduce the authentic grinding conditions used in OPC grinding. Instances of nanocrystallization and amorphization within clinker phases were hardly reported. In contrast, previous studies have

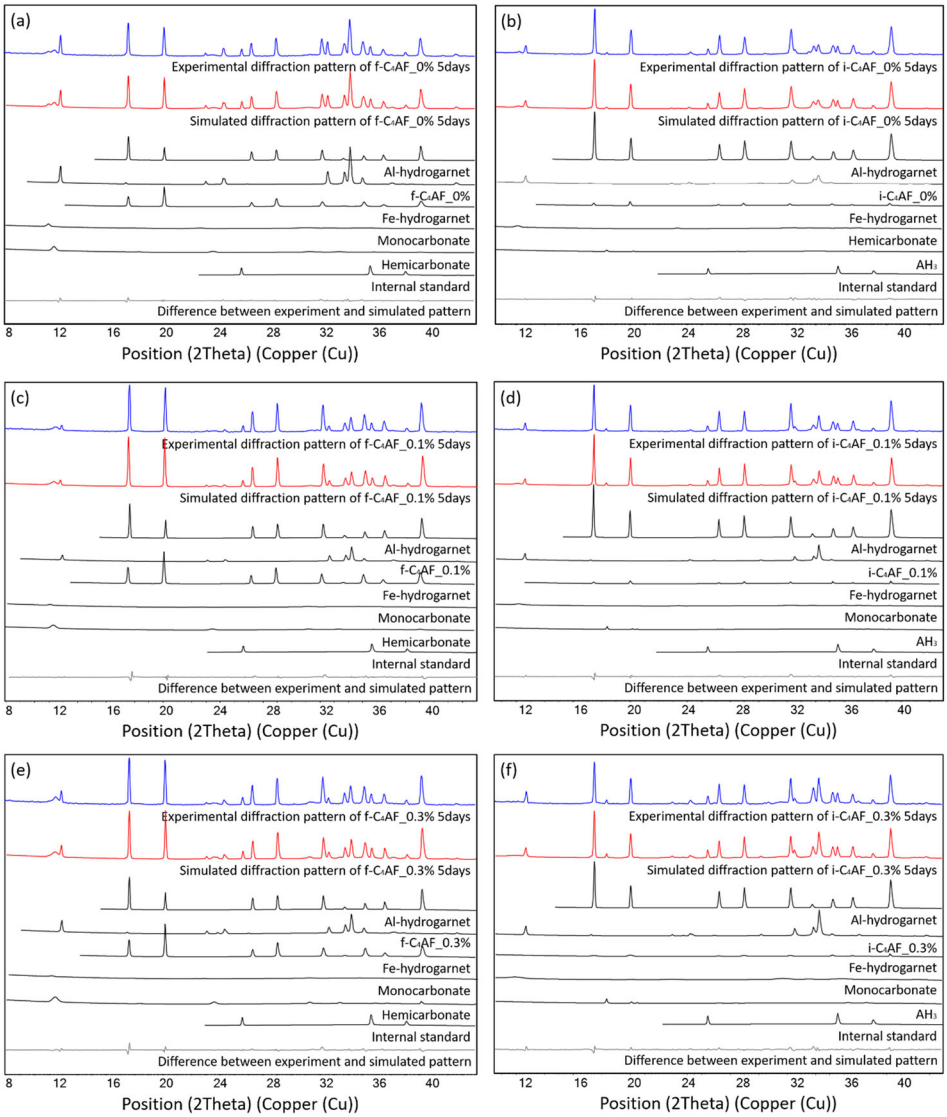

Figure 7. Quantitative phase analysis of XRD patterns of all investigated C_4AF (cured for 5 days): (a) f-C_4AF_0%, (b) i-C_4AF_0%, (c) f-C_4AF_0.1%, (d) i-C_4AF_0.1%, (e) f-C_4AF_0.3%, and (f) i-C_4AF_0.3%.

reported that the atomic arrangement within minerals can undergo partial modification due to grinding program [58–60]. Therefore, it indicates crystallographic modification since the addition of DEIPA contributed to the change in the unit cell parameters and the variations in the bond lengths of Fe-O and/or Al-O.

The profile-fitting results of the unhydrated C_4AF were presented in Table 6. The structural variations of C_4AF induced by DEIPA were confirmed regardless of the types of C_4AF phase and DEIPA content. Specifically, the unit cell parameters of C_4AF decreased according to the addition of DEIPA. The bond lengths of Fe-O and/or Al-O located in tetrahedral and octahedral configurations decreased. These variations could be closely related to the enhanced reactivity of C_4AF phases.

The relative quantitative analysis results of XPS are shown in Table 7 and Figure 10. When the DEIPA was added, the remarkable variations were observed in terms of the state of Fe atoms. In the case of f-C_4AF_0%, the relative fractions of Fe^{3+}/Fe^{2+} were calculated as 89.1%/10.9%, respectively. Meanwhile, with f-C_4AF_0.3%, the calculated value was 94.7%/5.3%, respectively. The large difference is mainly due to the peak of Fe^{3+} precursor. Thus, when DEIPA was added during the grinding procedure, it can be concluded that the large amount of Fe^{2+} transformed to the Fe^{3+} state.

As summarized, with DEIPA addition, the XRD patterns were significantly changed and resulted in the variations of crystal structure of C_4AF. Furthermore, the atomic state transition from Fe^{2+} to Fe^{3+} was also quantitatively measured *via* XPS. These results indicate that DEIPA acted as an oxidizing and activating agent for mainly Fe atoms in the C_4AF.

4.3. *Enhanced C_4AF hydration reaction due to DEIPA*

The QXRD results of all C_4AF (cured for 5 days) investigated are presented in Figure 11(a,b). When DEIPA was added, the improved degree of hydration was confirmed in f-C_4AF compared to the case of i-C_4AF. In the samples of f-C_4AF_0.1% and f-C_4AF_0.3%, the hydration products C_3FH_6 and Fe-Mc were significantly produced. In addition, amorphous content was significantly increased

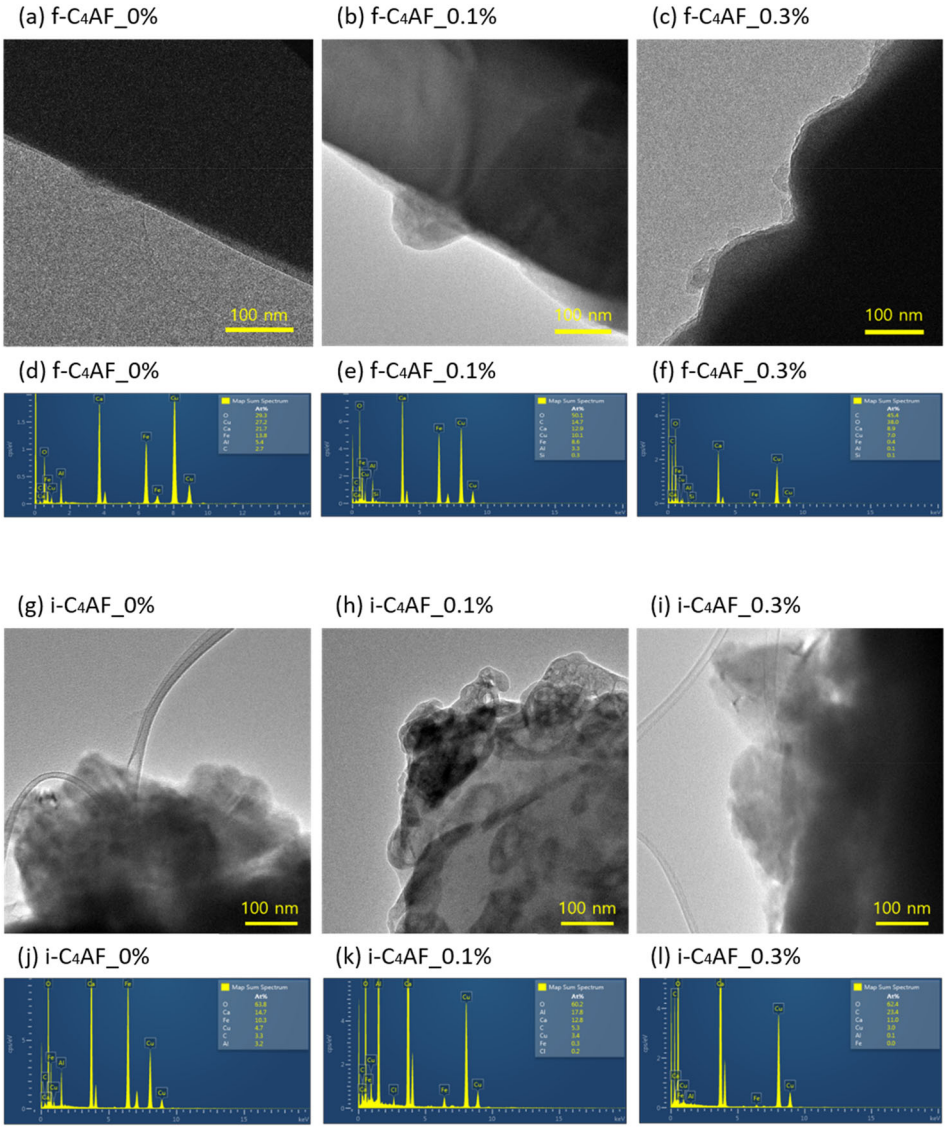

Figure 8. TEM and EDS measurement results for (a–f) f-C_4AF series and (g–l) i-C_4AF series.

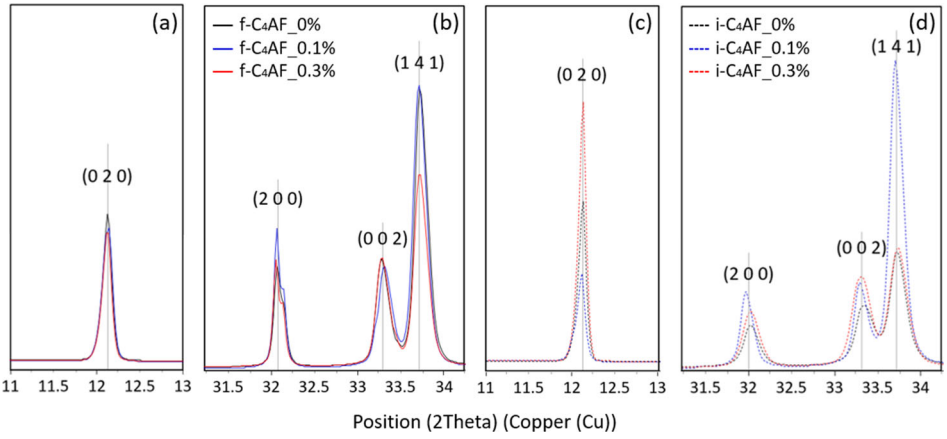

Figure 9. XRD measurements of (a–b) f-C_4AF and (c–d) i-C_4AF.

as the added amount of DEIPA increased. In previous studies, most of them was considered as amorphous Fe-containing phases [45, 61]. Thus, it was confirmed that Fe atoms contained in f-C_4AF significantly contributed to the hydration reaction.

Meanwhile, a different trend was observed in i-C_4AF. In the sample of i-C_4AF_0%, the Al-containing hydration products C_3AH_6, Al-Hc, and AH_3 were generated. However, when DEIPA was added, a completely different trend was confirmed in the hydration mechanism of i-C_4AF series. As the amount of DEIPA increased, C_3AH_6 decreased while the amount of amorphous increased significantly. Similar to the f-C_4AF, the reactivity of Fe atoms included in i-C_4AF was significantly

Table 6. Profile fitting results of unhydrated f-C_4AF and i-C_4AF.

	Unit cell parameters			Bond length of Fe/Al-O		
	a (Å)	b (Å)	c (Å)	Octahedral site (Å)	Tetrahedral site (Å)	Average (Å)
f-C_4AF_0%	5.5898	14.6304	5.3918	2.0417	1.7772	1.9359
f-C_4AF_0.1%	5.5860	14.6282	5.3855	2.0407	1.7763	1.9349
f-C_4AF_0.3%	5.5837	14.6261	5.3908	2.0407	1.7763	1.9349
i-C_4AF_0%	5.5786	14.5896	5.3682	2.0357	1.7720	1.9302
i-C_4AF_0.1%	5.5823	14.5687	5.3714	2.0353	1.7715	1.9298
i-C_4AF_0.3%	5.5693	14.5497	5.3630	2.0320	1.7683	1.9265

Table 7. Fitting results of f-C_4AF_0% and f-C_4AF_0.3%.

f-C_4AF_0%			f-C_4AF_0.3%		
Position (eV)	FWHM (eV)	Area (%)	Position (eV)	FWHM (eV)	Area (%)
706.8	2.2	61.5	706.1	2.2	55.3
709.0	2.8	27.6	707.8	3.2	35.6
714.0	4.4	10.9	710.5	1.6	3.8
–	–	–	714.0	3.0	5.3

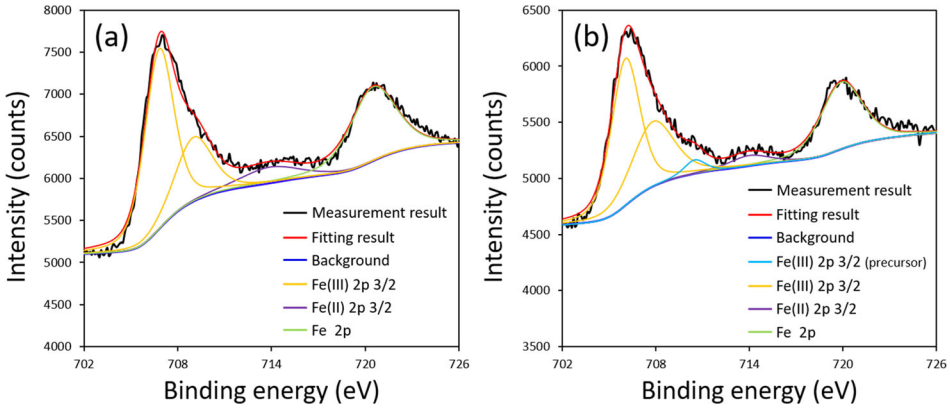

Figure 10. Quantification results of (a) f-C_4AF_0% and (b) f-C_4AF_0.3%.

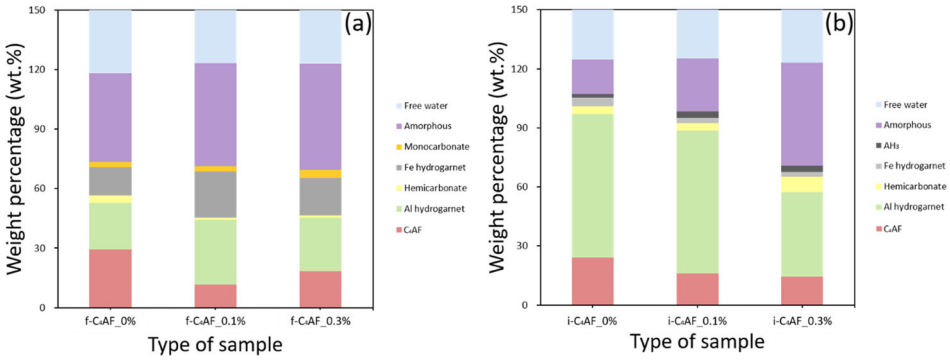

Figure 11. QXRD results of the (a) f-C_4AF and (b) i-C_4AF series cured for 5 days.

activated by the large amount addition of DEIPA. It also contributes to the production of amorphous phase consisting of Fe-containing phases (i.e. amorphous Fe-Mc, Fe-Hc, and FH_3). Consequently, enhanced reactivity of Fe source induced by DEIPA was confirmed regardless of the type of C_4AF phases.

The relationship between the measured amorphous content and particle size was presented in Figure 12(a,b). It is well-known fact that the particle surface area increased with decreasing particle size, resulting in higher reactivity [62]. In our study, a similar result was obtained; when the amount of DEIPA added increased from 0 to 0.1 wt.%, the quantified amorphous content was also increased. The highest grindability was achieved with a DEIPA dosage of 0.1 wt.%. However, an opposite trend was observed in the sample containing 0.3 wt.% of DEIPA. Although the grindability of f-C_4AF_0.3% and i-C_4AF_0.3% had not been enhanced, lots of amorphous Fe-containing hydration products were produced. From these results, it can be concluded that the further enhanced reactivity of the C_4AF was owing to the activated Fe atoms in C_4AF rather than the physical effect of particle size reduction.

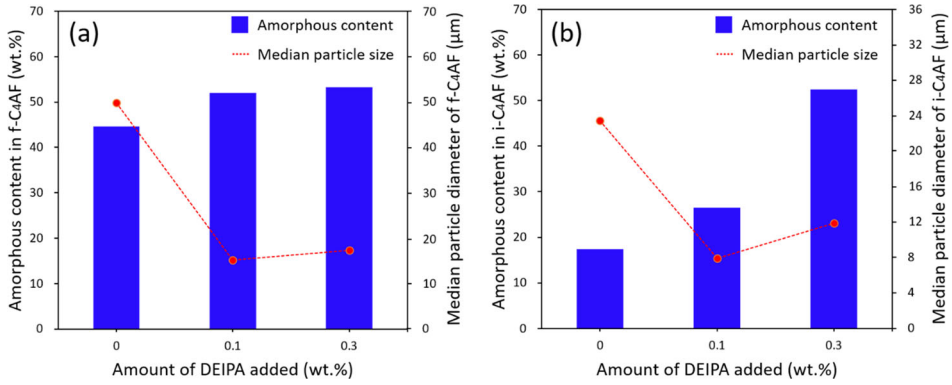

Figure 12. Relationship between QXRD (amorphous content) and effect of particle size variations: (a) the combination of f-C_4AF and DEIPA and (b) the combination of i-C_4AF and DEIPA.

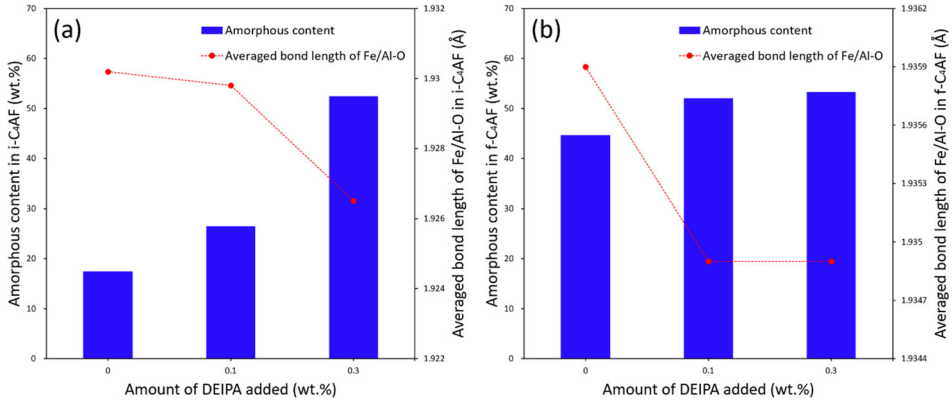

Figure 13. Relationship between amorphous content and bond length of (a) f-C_4AF and (b) i-C_4AF depending on the added DEIPA.

The quantified amount of amorphous content in the sample cured for 5 days could be associated with the crystallographic variations of the unhydrated C_4AF. When DEIPA was added, a change in the state of the Fe atoms observed in XPS (transformation from Fe^{2+} to Fe^{3+}) is reflected in the XRD pattern as the decreases of bond length of Fe/Al-O located in the C_4AF phase, which was shown in Figure 13(a,b). That is, the hydration reaction of C_4AF can be improved by the activated Fe^{3+} atoms, resulting in the decrease of bond length as well as the increased production of amorphous Fe containing AFm phase and FH_3.

5. Conclusions

In the current study, the crystallographic changes in C_4AF due to the DEIPA application during the grinding process were investigated using XRD, TEM, and XPS analyses. Modifications in the hydration characteristics due to the crystallographic variations were characterized by ICP-OES, isothermal calorimetry, TGA, and QXRD analyses. Two types of C_4AF (iron-rich $C_4A_{0.6}F_{1.4}$ (f-C_4AF) and idealized $C_4A_{0.8}F_{1.2}$ (i-C_4AF)) were synthesized and tested to evaluate the effect of DEIPA with dosages of 0, 0.1, and 0.3 wt.%. The conclusions of this study are as follows:

The significant particle size reduction (i.e. enhanced grindability) of C_4AF was confirmed by the addition of DEIPA. In particular, this effect was more pronounced in C_4AF_0.1% than in the case of C_4AF_0.3%. High-volume energy introduced by the grinding program mainly contributed to the size reduction of C_4AF_0.1% whereas the energy would have been much used to change the crystallographic structure of C_4AF_0.3%. Furthermore, uneven surface of f-C_4AF particle was observed *via* TEM with the addition of DEIPA.

Through XRD and XPS analyses, the state variations of Fe atoms in C_4AF were confirmed. Not only did the transformation from Fe^{2+} to Fe^{3+} occur, but the variation of crystallographic information of Fe-O and/or Al-O was also identified. These two observations support the origin of enhanced hydration reaction of C_4AF. The enhanced reaction produces large amounts of Fe containing phases such as Fe-AFm and amorphous FH_3. This is more pronounced in f-C_4AF phase. In the case of i-C_4AF phase, similar enhancement was only observed by the large amount of usage of DEIPA of 0.3 wt.%.

Therefore, it can be concluded that the reactivity of Fe atoms in C_4AF was substantially improved by the small addition of DEIPA during grinding process. The degree of enhanced reactivity can be also tailored by the dosage of the DEIPA considering the nature of the C_4AF phase in various cement-based mixtures. The findings in this study can be used to design and develop sustainable PC such as ferrite-rich PC or improved performance of conventional PC system.

Acknowledgements

This work was supported by Korea Institute of Energy Technology Evaluation and Planning (KETEP) grant funded by the Korea government (MOTIE) (20212010200080, Development of In-situ carbonation technology using CO2 released from cement industry). The Institute of Engineering Research at Seoul National University provided research facilities for this work. The authors also thank Yuna Bae, Jihoon Kim, and Hayoung Park at SNU CBE for help with TEM measurement.

Disclosure statement

No potential conflict of interest was reported by the author(s).

References

[1] Phan T-L, Tran N, Kim DH, et al. Electronic structure and magnetic properties of Al-doped Ca2Fe2O5 brownmillerite compounds. J Am Ceram Soc. 2018;101(5):2181–2189. doi: 10.1111/jace.15357.

[2] Tao Y, Wan D, Zhang W, et al. Intrinsic reactivity and dissolution characteristics of tetracalcium aluminoferrite. Cem Concr Res. 2021;146:106485. doi: 10.1016/j.cemconres.2021.106485.

[3] Aranda MAG, De la Torre AG, Leon-Reina L. Rietveld quantitative phase analysis of OPC clinkers, cements and hydration products. Rev Mineral Geochem. 2012;74(1):169–209. doi: 10.2138/rmg.2012.74.5.

[4] Jeffery J. The crystal structure of tricalcium silicate. Acta Cryst. 1952;5(1):26–35. doi: 10.1107/S0365110X52000083.

[5] Zhao R, Zhang L, Fan G, et al. Probing the exact form and doping preference of magnesium in ordinary Portland cement clinker phases: a study from experiments and DFT simulations. Cem Concr Res. 2021;144:106420. doi: 10.1016/j.cemconres.2021.106420.

[6] Zhang K, Shen P, Yang L, et al. Development of high-ferrite cement: toward green cement production. J Cleaner Prod. 2021;327:129487. doi: 10.1016/j.jclepro.2021.129487.

[7] Meller N, Hall C, Jupe AC, et al. The paste hydration of brownmillerite with and without gypsum: a time resolved synchrotron diffraction study at 30, 70, 100 and 150 C. J Mater Chem. 2004;14(3):428–435. doi: 10.1039/B313215C.

[8] Di Filippo J, Karpman J, DeShazo J. The impacts of policies to reduce CO2 emissions within the concrete supply chain. Cem Concr Compos. 2019;101:67–82. doi: 10.1016/j.cemconcomp.2018.08.003.

[9] Elakneswaran Y, Noguchi N, Matumoto K, et al. Characteristics of ferrite-rich Portland cement: comparison with ordinary Portland cement. Front Mater. 2019;6:97. doi: 10.3389/fmats.2019.00097.

[10] Gartner E, Myers D. Influence of tertiary alkanolamines on Portland cement hydration. J Am Ceramic Soc. 1993;76(6):1521–1530. doi: 10.1111/j.1151-2916.1993.tb03934.x.

[11] Ramachandran VS. Hydration of cement—role of triethanolamine. Cem Concr Res. 1976;6(5):623–631. doi: 10.1016/0008-8846(76)90026-0.

[12] Yilmaz VT, Menek N, Odabasoğlu M. Quantitative determination of triethanolamine in cements. Cem Concr Res. 1993;23(3):603–608. doi: 10.1016/0008-8846(93)90011-W.

[13] Heren Z, Ölmez H. The influence of ethanolamines on the hydration and mechanical properties of Portland cement. Cem Concr Res. 1996;26(5):701–705. doi: 10.1016/S0008-8846(96)85007-1.

[14] Katsioti M, Tsakiridis PE, Giannatos P, et al. Characterization of various cement grinding aids and their impact on grindability and cement performance. Constr Build Mater. 2009;23(5):1954–1959. doi: 10.1016/j.conbuildmat.2008.09.003.

[15] Toprak NA, Benzer AH, Karahan CE, et al. Effects of grinding aid dosage on circuit performance and cement fineness. Constr Build Mater. 2020;265:120707. doi: 10.1016/j.conbuildmat.2020.120707.

[16] Sun Z, Yang H, Shui L, et al. Preparation of polycarboxylate-based grinding aid and its influence on cement properties under laboratory condition. Constr Build Mater. 2016;127:363–368. doi: 10.1016/j.conbuildmat.2016.10.007.

[17] Cheung J, Jeknavorian A, Roberts L, et al. Impact of admixtures on the hydration kinetics of Portland cement. Cem Concr Res. 2011;41(12):1289–1309. doi: 10.1016/j.cemconres.2011.03.005.

[18] Sandberg PJ, Doncaster F. On the mechanism of strength enhancement of cement paste and mortar with triisopropanolamine. Cem Concr Res. 2004;34(6):973–976. doi: 10.1016/j.cemconres.2003.11.018.

[19] Ma S, Li W, Zhang S, et al. Study on the hydration and microstructure of Portland cement containing diethanol-isopropanolamine. Cem Concr Res. 2015;67:122–130. doi: 10.1016/j.cemconres.2014.09.002.

[20] Lu Z, Kong X, Jansen D, et al. Towards a further understanding of cement hydration in the presence of triethanolamine. Cem Concr Res. 2020;132:106041. doi: 10.1016/j.cemconres.2020.106041.

[21] Huang H, Wang Q, Li X, et al. Sulfate adjustment for cement with triisopropanolamine: mechanism of early strength enhancement. Constr Build Mater. 2018;182:516–522. doi: 10.1016/j.conbuildmat.2018.06.123.

[22] Wesselsky A, Jensen OM. Synthesis of pure Portland cement phases. Cem Concr Res. 2009;39(11):973–980. doi: 10.1016/j.cemconres.2009.07.013.

[23] Snellings R, Bazzoni A, Scrivener K. The existence of amorphous phase in Portland cements: physical factors affecting rietveld quantitative phase analysis. Cem Concr Res. 2014;59:139–146. doi: 10.1016/j.cemconres.2014.03.002.

[24] Delhaye D, Ouf F-X, Ferry D, et al. The MERMOSE project: characterization of particulate matter emissions of a commercial aircraft engine. J Aerosol Sci. 2017;105:48–63. doi: 10.1016/j.jaerosci.2016.11.018.

[25] Claes N, Asapu R, Blommaerts N, et al. *Characterization of silver-polymer core–shell nanoparticles using electron microscopy*. Nanoscale. 2018;10(19):9186–9191. doi: 10.1039/c7nr09517a.

[26] Mei K, Cheng X, Gu T, et al. Effects of Fe and Al ions during hydrogen sulphide (H2S)-induced corrosion of tetracalcium aluminoferrite (C4AF) and tricalcium aluminate (C3A). J Hazard Mater. 2021;403:123928. doi: 10.1016/j.jhazmat.2020.123928.

[27] Yamashita T, Hayes P. Analysis of XPS spectra of Fe2+ and Fe3+ ions in oxide materials. Appl Surf Sci. 2008;254(8):2441–2449. doi: 10.1016/j.apsusc.2007.09.063.

[28] Caruso F, Mantellato S, Palacios M, et al. ICP-OES method for the characterization of cement pore solutions and their modification by polycarboxylate-based superplasticizers. Cem Concr Res. 2017;91:52–60. doi: 10.1016/j.cemconres.2016.10.007.

[29] Maheswaran S, Kalaiselvam S, Saravana Karthikeyan SKS, et al. β-Belite cements (β-dicalcium silicate) obtained from calcined lime sludge and silica fume.

Cem Concr Compos. 2016;66:57–65. doi: 10.1016/j.cemconcomp.2015.11.008.
[30] Jeong Y, Kang S-H, Kim MO, et al. Acceleration of cement hydration from supplementary cementitious materials: performance comparison between silica fume and hydrophobic silica. Cem Concr Compos. 2020;112:103688. doi: 10.1016/j.cemconcomp.2020.103688.
[31] Kang H, Moon J. Secondary curing effect on the hydration of ultra-high performance concrete. Constr Build Mater. 2021;298:123874. doi: 10.1016/j.conbuildmat.2021.123874.
[32] Jeong Y, Hargis CW, Kang H, et al. The effect of elevated curing temperatures on high ye'elimite calcium sulfoaluminate cement mortars. Materials. 2019;12(7):1072. doi: 10.3390/ma12071072.
[33] Finger L, Cox D, Jephcoat A. A correction for powder diffraction peak asymmetry due to axial divergence. J Appl Crystallogr. 1994;27(6):892–900. doi: 10.1107/S0021889894004218.
[34] Gualtieri A, Norby P, Hanson J, et al. Rietveld refinement using synchrotron X-ray powder diffraction data collected in transmission geometry using an imaging-plate detector: application to standard m-ZrO2. J Appl Crystallogr. 1996;29(6):707–713. doi: 10.1107/S0021889896008199.
[35] Kim H, Lee S, Park Y-U, et al. Neutron and X-ray diffraction study of pyrophosphate-based Li2–x MP2O7 (M = Fe, Co) for lithium rechargeable battery electrodes. Chem Mater. 2011;23(17):3930–3937. doi: 10.1021/cm201305z.
[36] Kang H, Lee N, Moon J. Elucidation of the hydration reaction of UHPC using the PONKCS method. Materials. 2020;13(20):4661. doi: 10.3390/ma13204661.
[37] Howard BH. Preliminary data on QXRD analysis of Portland cement and clinker using CeO2 as the internal standard. Cem Concr Res. 1984;14(5):729–740. doi: 10.1016/0008-8846(84)90036-X.
[38] Colville A, Geller S. The crystal structure of brownmillerite, Ca2FeAlO5. Acta Crystallogr B Struct Crystallogr Cryst Chem. 1971;27(12):2311–2315. doi: 10.1107/S056774087100579X.
[39] Lager GA, Downs RT, Origlieri M, et al. High-pressure single-crystal X-ray diffraction study of katoite hydrogarnet: evidence for a phase transition from Ia 3 d→ I $\bar{4}$3 d symmetry at 5 GPa. Am Mineral. 2002;87(5–6):642–647. doi: 10.2138/am-2002-5-606.
[40] Dilnesa BZ, Lothenbach B, Le Saout G, et al. Iron in carbonate containing AFm phases. Cem Concr Res. 2011;41(3):311–323. doi: 10.1016/j.cemconres.2010.11.017.
[41] François M, Renaudin G, Evrard O. A cementitious compound with composition 3CaO. Al2O3. CaCO3. 11H2O. Acta Crystallogr C: Crystal Struct Commun. 1998;54(9):1214–1217.
[42] Runčevski T, Dinnebier RE, Magdysyuk OV, et al. Crystal structures of calcium hemicarboaluminate and carbonated calcium hemicarboaluminate from synchrotron powder diffraction data. Acta Crystallogr B. 2012;68(Pt 5):493–500. doi: 10.1107/S010876811203042X.
[43] Saalfeld H, Wedde M. Refinement of the crystal structure of gibbsite, A1 (OH) 3. Zeitschrift Für Kristallographie-Crystal Mater. 1974;139(1–6):129–135. doi: 10.1524/zkri.1974.139.16.129.
[44] Zhang G, Ren Q, He J, et al. New understanding of early hydration of C4AF under surface vitrification. Powder Technol. 2021;377:372–378. doi: 10.1016/j.powtec.2020.08.098.
[45] Cuesta A, Santacruz I, Sanfélix SG, et al. Hydration of C4AF in the presence of other phases: a synchrotron X-ray powder diffraction study. Constr Build Mater. 2015;101:818–827. doi: 10.1016/j.conbuildmat.2015.10.114.
[46] Przwara P, Kwade A. Grinding aid additives for dry fine grinding processes–part II: continuous and industrial grinding. Powder Technol. 2021;394:207–213. doi: 10.1016/j.powtec.2021.08.039.
[47] Kumar S, Bandopadhyay A, Rajinikanth V, et al. Improved processing of blended slag cement through mechanical activation. J Mater Sci. 2004;39(10):3449–3452. doi: 10.1023/B:JMSC.0000026948.85440.cc.
[48] Tafesse M, Lee HK, Alemu AS, et al. On the expansive cracking of a cement matrix containing atomized basic oxygen furnace slag with a metallic iron. Constr Build Mater. 2020;264:119806. doi: 10.1016/j.conbuildmat.2020.119806.
[49] Roosendaal SJ, van Asselen B, Elsenaar JW, et al. The oxidation state of Fe (100) after initial oxidation in O2. Surf Sci. 1999;442(3):329–337. doi: 10.1016/S0039-6028(99)01006-7.
[50] Graat PC, Somers MA. Simultaneous determination of composition and thickness of thin iron-oxide films from XPS Fe 2p spectra. Appl Surf Sci. 1996;100–101:36–40. doi: 10.1016/0169-4332(96)00252-8.
[51] Mekki A, Holland D, McConville CF, et al. An XPS study of iron sodium silicate glass surfaces. J Non-Cryst Solids. 1996;208(3):267–276. doi: 10.1016/S0022-3093(96)00523-6.
[52] Chang J, Zhang Y, Shang X, et al. Effects of amorphous AH3 phase on mechanical properties and hydration process of C4A3S\bar-CS\bar H2-CH-H2O system. Constr Build Mater. 2017;133:314–322. doi: 10.1016/j.conbuildmat.2016.11.111.
[53] MacKenzie K, Temuujin J, Okada K. Thermal decomposition of mechanically activated gibbsite. Thermochim Acta. 1999;327(1–2):103–108. doi: 10.1016/S0040-6031(98)00609-1.
[54] Vernekar D, Jagadeesan D. Tunable acid–base bifunctional catalytic activity of FeOOH in an orthogonal tandem reaction. Catal Sci Technol. 2015;5(8):4029–4038. doi: 10.1039/C5CY00361J.
[55] Li M, Li B, Meng F, et al. Highly sensitive and selective butanol sensors using the intermediate state nanocomposites converted from β-FeOOH to α-Fe2O3. Sens Actuators, B. 2018;273:543–551. doi: 10.1016/j.snb.2018.06.081.
[56] Aman AK, et al. Effect of superfine grinding on structural, morphological and antioxidant properties of ginger (Zingiber officinale) nano crystalline food powder. Mater Today: Proc. 2021;43:3397–3403.
[57] Huang Z-Q, Xie X-L, Chen Y, et al. Ball-milling treatment effect on physicochemical properties and features for cassava and maize starches. CR Chim. 2008;11(1–2):73–79. doi: 10.1016/j.crci.2007.04.008.
[58] Dey JK, Chatterjee A, Majumdar S, et al. Ferroelectric order associated with ordered occupancy at the octahedral site of the inverse spinel structure of multiferroic NiFe 2 O 4. Phys Rev B. 2019;99(14):144412. pdoi: 10.1103/PhysRevB.99.144412.
[59] Kojdecki MA, Bastida J, Pardo P, et al. Crystalline microstructure of sepiolite influenced by grinding. J Appl Crystallogr. 2005;38(6):888–899. doi: 10.1107/S0021889805026476.
[60] Kristof E, Juhász A. The effect of intensive grinding on the crystal structure of dolomite. Powder Technol. 1993;75(2):145–152. doi: 10.1016/0032-5910(93)80075-L.
[61] Deng Q, Zhao M, Rao M, et al. Effect of CuO-doping on the hydration mechanism and the chloride-binding capacity of C4AF and high ferrite Portland clinker. Constr Build Mater. 2020;252:119119. doi: 10.1016/j.conbuildmat.2020.119119.
[62] He Y, Liu S, Luo Q, et al. Influence of PCE-type GA on cement hydration performances. Constr Build Mater. 2021;302:124432. doi: 10.1016/j.conbuildmat.2021.124432.